This paper is published as part of Faraday Discussions volume 141:

Water – From Interfaces to the Bulk

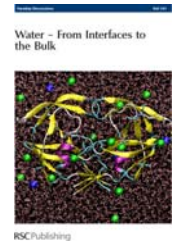

Introductory Lecture

Spiers Memorial Lecture

Ions at aqueous interfaces

Pavel Jungwirth, *Faraday Discuss.*, 2009

DOI: 10.1039/b816684f

Papers

The surface of neat water is basic

James K. Beattie, Alex M. Djerdjev and Gregory G. Warr, *Faraday Discuss.*, 2009

DOI: 10.1039/b805266b

Negative charges at the air/water interface and their consequences for aqueous wetting films containing surfactants

Katarzyna Hänni-Ciunel, Natascha Schelero and Regine von Klitzing, *Faraday Discuss.*, 2009

DOI: 10.1039/b809149h

Water-mediated ordering of nanoparticles in an electric field

Dusan Bratko, Christopher D. Daub and Alenka Luzar, *Faraday Discuss.*, 2009

DOI: 10.1039/b809135h

Ultrafast phase transitions in metastable water near liquid interfaces

Oliver Link, Esteban Vöhringer-Martinez, Eugen Lugovoj, Yaxing Liu, Katrin Siefermann, Manfred Faubel, Helmut Grubmüller, R. Benny Gerber, Yifat Miller and Bernd Abel, *Faraday Discuss.*, 2009

DOI: 10.1039/b811659h

Discussion

General discussion

Faraday Discuss., 2009

DOI: 10.1039/b818382c

Papers

Hydration dynamics of purple membranes

Douglas J. Tobias, Neelanjana Sengupta and Mounir Tarek, *Faraday Discuss.*, 2009

DOI: 10.1039/b809371g

From shell to cell: neutron scattering studies of biological water dynamics and coupling to activity

A. Frölich, F. Gabel, M. Jasnin, U. Lehnert, D. Oesterhelt, A. M. Stadler, M. Tehei, M. Weik, K. Wood and G. Zaccai, *Faraday Discuss.*, 2009

DOI: 10.1039/b805506h

Time scales of water dynamics at biological interfaces: peptides, proteins and cells

Johan Qvist, Erik Persson, Carlos Mattea and Bertil Halle, *Faraday Discuss.*, 2009

DOI: 10.1039/b806194g

Structure and dynamics of interfacial water in model lung surfactants

Avishek Ghosh, R. Kramer Campen, Maria Sovago and Mischa Bonn, *Faraday Discuss.*, 2009

DOI: 10.1039/b805858j

The terahertz dance of water with the proteins: the effect of protein flexibility on the dynamical hydration shell of ubiquitin

Benjamin Born, Seung Joong Kim, Simon Ebbinghaus, Martin Gruebele and Martina Havenith, *Faraday Discuss.*, 2009

DOI: 10.1039/b804734k

Discussion

General discussion

Faraday Discuss., 2009

DOI: 10.1039/b818384h

Papers

Coarse-grained modeling of the interface between water and heterogeneous surfaces

Adam P. Willard and David Chandler, *Faraday Discuss.*, 2009

DOI: 10.1039/b805786a

Water growth on metals and oxides: binding, dissociation and role of hydroxyl groups

M. Salmeron, H. Bluhm, M. Tatarkhanov, G. Ketteler, T. K. Shimizu, A. Mugarza, Xingyi Deng, T. Herranz, S. Yamamoto and A. Nilsson, *Faraday Discuss.*, 2009

DOI: 10.1039/b806516k

Order and disorder in the wetting layer on Ru(0001)

Mark Gallagher, Ahmed Omer, George R. Darling and Andrew Hodgson, *Faraday Discuss.*, 2009

DOI: 10.1039/b807809b

What ice can teach us about water interactions: a critical comparison of the performance of different water models

C. Vega, J. L. F. Abascal, M. M. Conde and J. L. Aragones, *Faraday Discuss.*, 2009

DOI: 10.1039/b805531a

On thin ice: surface order and disorder during pre-melting

C. L. Bishop, D. Pan, L. M. Liu, G. A. Tribello, A. Michaelides, E. G. Wang and B. Slater, *Faraday Discuss.*, 2009

DOI: 10.1039/b807377p

Reactivity of water–electron complexes on crystalline ice surfaces

Mathieu Bertin, Michael Meyer, Julia Stähler, Cornelius Gahl, Martin Wolf and Uwe Bovensiepen, *Faraday Discuss.*, 2009

DOI: 10.1039/b805198d

Discussion

General discussion

Faraday Discuss., 2009

DOI: 10.1039/b818385f

Papers

Similarities" between confined and supercooled water

Maria Antonietta Ricci, Fabio Bruni and Alessia Giuliani, *Faraday Discuss.*, 2009

DOI: 10.1039/b805706k

Structural and mechanical properties of glassy water in nanoscale confinement

Thomas G. Lombardo, Nicolás Giovambattista and Pablo G. Debenedetti, *Faraday Discuss.*, 2009

DOI: 10.1039/b805361h

Water nanodroplets confined in zeolite pores

François-Xavier Coudert, Fabien Cailliez, Rodolphe Vuilleumier, Alain H. Fuchs and Anne Boutin, *Faraday Discuss.*, 2009

DOI: 10.1039/b804992k

Dynamic properties of confined hydration layers

Susan Perkin, Ronit Goldberg, Liraz Chai, Nir Kampf and Jacob Klein, *Faraday Discuss.*, 2009

DOI: 10.1039/b805244a

Study of a nanoscale water cluster by atomic force microscopy

Manhee Lee, Baekman Sung, N. Hashemi and Wonho Jhe, *Faraday Discuss.*, 2009

DOI: 10.1039/b807740c

Water at an electrochemical interface—a simulation study

Adam P. Willard, Stewart K. Reed, Paul A. Madden and David Chandler, *Faraday Discuss.*, 2009

DOI: 10.1039/b805544k

Discussion

General discussion

Faraday Discuss., 2009

DOI: 10.1039/b818386b

Concluding remarks

Concluding remarks

Peter J. Feibelman, *Faraday Discuss.*, 2009

DOI: 10.1039/b817311g

Structural and mechanical properties of glassy water in nanoscale confinement

Thomas G. Lombardo, Nicolás Giovambattista and Pablo G. Debenedetti*

Received 1st April 2008, Accepted 16th May 2008
First published as an Advance Article on the web 25th September 2008
DOI: 10.1039/b805361h

We investigate the structure and mechanical properties of glassy water confined between silica-based surfaces with continuously tunable hydrophobicity and hydrophilicity by computing and analyzing minimum energy, mechanically stable configurations (inherent structures). The structured silica substrate imposes long-range order on the first layer of water molecules under hydrophobic confinement at high density ($\rho \geq 1.0$ g cm^{-3}). This proximal layer is also structured in hydrophilic confinement at very low density ($\rho \sim 0.4$ g cm^{-3}). The ordering of water next to the hydrophobic surface greatly enhances the mechanical strength of thin films (0.8 nm). This leads to a substantial stress anisotropy; the transverse strength of the film exceeds the normal strength by 500 MPa. The large transverse strength results in a minimum in the equation of state of the energy landscape that does not correspond to a mechanical instability, but represents disruption of the ordered layer of water next to the wall. In addition, we find that the mode of mechanical failure is dependent on the type of confinement. Under large lateral strain, water confined by hydrophilic surfaces preferentially forms voids in the middle of the film and fails cohesively. In contrast, water under hydrophobic confinement tends to form voids near the walls and fails by loss of adhesion.

1 Introduction

Water is the most abundant substance on the Earth's surface, of which it covers approximately 70%.[1] There is hardly a human activity from agriculture to travel and from manufacture to artistic creation that is not dependent on, influenced or inspired by the properties of water. Life itself as we know it depends on water (see *e.g.* ref. 2–5). About 70% of human body weight is water, and 70% of this water is found in intracellular fluid.[6] Thus, most biochemical processes such as protein synthesis occur in aqueous solution. It has been proposed that water be considered as 'an integral and active component of biomolecular systems' rather than as an 'inert environment'.[7] To the physical scientist, water remains a source of continued interest and curiosity on account of its many anomalous properties. The peculiar behavior of many of water's properties, which render it qualitatively different from most other substances, becomes more pronounced at low temperature.[8–10] In the liquid phase, examples include the increase of the isothermal compressibility upon isobaric cooling[11] and the enhancement of diffusivity upon isothermal compression.[12] In the glass state, water exhibits polyamorphism, existing in at least two different forms,[13–16] which may be separated by a first-order transition.[8,17] Understanding the molecular basis of this complex behavior remains an active area of research.[17]

Department of Chemical Engineering, Princeton University, Princeton, New Jersey, USA. E-mail: pdebene@princeton.edu

In many situations, water is found in confined geometries or as a thin film in contact with surfaces. Examples are numerous, encompassing fields such as geology (*e.g.* in zeolites[18] and mineral inclusions[19]) as well as technological applications (*e.g.* in nanofluidics[20,21] and cryopreservation[22]). Understanding the behavior of confined and interfacial water is particularly important in biology. The cell interior is a crowded environment where proteins are separated on average by 2–3 water layers.[23] The dynamics of proteins in such an environment is tightly correlated with water dynamics.[24] Water's behavior under confinement is incompletely understood, depending sensitively on the properties of the confining surfaces such as surface hydrophilicity,[25–27] chemical heterogeneity[28] and topography.[29,30] Recent experiments that attempt to shed light on supercooled water's bulk properties from measurements performed in nanoscopic pores[31,32] highlight the importance of understanding water's properties in the presence of confining surfaces.[33–35]

The characterization of confined water properties at low temperature (either in the glass state, or close to the system's glass transition temperature, T_g) is particularly relevant in pharmaceutical applications.[36–39] This is primarily because one of the most common techniques to preserve pharmaceuticals, including proteins as well as small-molecular-weight drugs and peptides, is lyophilization.[37] Lyophilization is the process of freezing the substance to be stored into an amorphous state, followed by drying.[40] In addition to the substance to be preserved, lyophilized formulations consist of a glassy matrix[41] composed typically of sugars with up to 4% by weight of water, plus excipients such as fillers and anti-oxidants.[42,43] Cooling the system into the glassy state greatly reduces the rate of transport processes, thereby protecting proteins or other labile biochemicals against aggregation or chemical reactions which can otherwise damage the product.[37,44–46] The drying process consists of sublimation of water from the glassy matrix: water is a good plasticizer and unless its concentration is kept sufficiently low it will greatly facilitate molecular mobility.[47–51] Although lyophilization is commonly used in the pharmaceutical and food processing industries, it is incompletely understood at the molecular level. Lyophilization generates both freezing and drying stresses. These stresses, as well as aging in the glass state, can result in undesired molecular mobility.[36,37,52,53] Such residual stresses are intimately related to the way in which water behaves under confinement and at extended interfaces with large solutes, such as proteins, both in the glass state and as the system is cooled from the liquid phase across T_g.

Ice formation inside the cell is injurious and can be lethal for organisms living in subfreezing conditions.[54] One strategy for survival at these conditions involves depressing water's freezing point.[55] Alternatively, ice nucleation can be inhibited kinetically by antifreeze proteins, such as those commonly found in Antarctic fish,[56] and also observed in insects at low temperature.[57] The mechanisms by which biological surfaces can suppress ice nucleation are poorly understood.

Cold water close to biological surfaces is believed to play an important role in the low-temperature unfolding of proteins.[58] This process, which is the subject of much current interest (see *e.g.* ref. 59 and 60), is believed to have important implications for the possibility of life at extreme conditions.[61] Finally, we mention the fact that thin films of glassy water have played an important role in the ongoing quest to understand the thermodynamics of deeply supercooled bulk water.[62–65]

The selected examples above illustrate the importance of understanding the behavior of supercooled and glassy water in confinement. Here, we are specifically interested in confined glassy water, and we take a step in this direction by exploring the structure and mechanical properties of amorphous solid water confined between two parallel silica-based nanoscale surfaces separated by $d = 0.8$ and 1.6 nm. We consider a family of surfaces with tunable hydrophilicity and study glassy water configurations obtained by energy minimization (inherent structures[66]). We explore the effect of d and surface hydrophilicity on water stresses and on the amorphous films' mechanical failure modes. The picture that emerges is quite rich. Water responds to lateral strain, surface chemistry and confinement in ways that include

the formation of layered phases with unusually large mechanical strength, and the appearance of surface-chemistry-sensitive failure modes. It is therefore anticipated that future similar studies, but with the added complexities of biologically-relevant confining surfaces[67] and carbohydrates, will provide valuable insights into the mechanisms underlying the preservation of labile biomolecules in glassy matrices.

The present work was inspired by recent theoretical and computational studies of atomic glassy films using the potential-energy landscape formalism.[68–70] We also note the recent related study of inherent structures of a confined Lennard-Jones binary mixture by Attili *et al.*[71] This paper is organized as follows. Section 2 provides details on the molecular simulation and energy minimization techniques and specifies the various systems studied. Analysis and results of glassy configurations of confined water are presented and discussed in section 3. The major conclusions arrived at in this work and the open questions arising as a result of our study are listed in section 4.

2 Simulation methods

A powerful framework for examining liquids and glasses is the potential-energy landscape (PEL) approach. The basic concepts of the PEL originate in the work of Goldstein, more than 30 years ago.[72,73] Stillinger and Weber incorporated these ideas into a mathematical theory that placed the PEL interpretation on firm conceptual ground.[66,74] The PEL is the hypersurface defined by the potential energy (PE) of the system as a function of its degrees of freedom. For a given system composed of N particles in a fixed volume, there exist $(3 + n)N$ degrees of freedom. Each particle is specified by three center-of-mass (CM) coordinates and n orientational, vibrational and conformational degrees of freedom. The PEL is the potential-energy hypersurface in $[(3 + n)N + 1]$-dimensional space, and the system configuration is represented by a single point on the surface. This multidimensional surface cannot be visualized, but the local minima and potential-energy barriers between them are often characterized with three-dimensional descriptions such as peaks, basins and ridges. As the particles of the system move, the representative point of the system on the PEL also moves.[66,75,76] For the case of high-temperature liquids, kinetic energy allows the system to visit most of the basins. However, as the temperature is reduced, potential-energy barriers become relevant and the number of basins accessible to the system decreases. Upon further cooling, the system becomes trapped in a single basin, entering the glassy state. Here we use the term basin to denote the collection of configurations that are mapped onto the same local minimum (or its $N!$ permutationally identical versions obtained by particle interchanges) upon energy minimization.

Computationally, glassy configurations can be generated by two methods: rapid cooling and potential-energy minimization (which can be regarded as the infinite-cooling-rate limit of the former process). This study focuses on the latter approach, and in particular on inherent structures (IS), the local minima of the PEL. Inherent structures are calculated by minimizing the potential energy of an equilibrium configuration with respect to all of its degrees of freedom. The local minima of the PEL are mechanically stable packings that in principle lack long-range order, and are hence representative of glasses.

We analyze the effects of wall-to-wall separation, density and surface chemistry for glassy water confined between two parallel plates. Water is modeled with the extended simple-point-charge (SPC/E) model: a rigid three-site representation of water with a tetrahedral bond angle and partial charges at the oxygen and hydrogen sites, in addition to Lennard-Jones (LJ) dispersive interactions between oxygen atoms.[77] The properties of bulk SPC/E water have been studied extensively in the liquid and glassy states, and the model exhibits many of water's anomalies.[78–80] We confine water between two parallel atomically detailed silica-based walls with force fields developed by Lee and Rossky;[81] these walls have been used in several recent studies to examine the hydration and phase behavior of water under

confinement.[27,28,82] The underlying structure of the confining walls consists of four layers of SiO_2 which reproduce the (111) octahedral face of cristobalite.

The unit cell of the silica-based walls is an idealized tetrahedron with O–O and Si–O distances of 0.247 nm and 0.151 nm respectively. All Si and O wall atoms interact with the O atom of water molecules *via* a LJ interaction. When only LJ interactions are present, the surface displays a hydrophobic character;[82] to increase the plate's affinity for water the surface of each plate is fully hydroxylated, producing charged Si–O–H groups with a bond angle of 109.27°. These charged Si, O and H atoms exist only at the surface of the wall and have Coulombic interactions with the three charged sites on each SPC/E water molecule; the addition of electrostatic interactions creates a hydrophilic surface.[27,28,82] The Si and O atoms are fixed, but the H atoms are allowed to move with fixed O–H length and Si–O–H bond angle; the motion of each H atom therefore traces a circle parallel to the wall. The LJ parameters for all Si and O wall atoms, and the charges for surface Si–O–H atoms are given in Table 1. All LJ interactions, including those between O atoms of SPC/E water molecules, are truncated at 0.79 nm with a switching function such that the potential and its first two derivatives are zero at the cutoff.[83] This is essential for the system to be amenable to energy minimization techniques used to generate glassy configurations (see below). More details about the walls can be found in ref. 81 and 82.

Most natural surfaces have interactions with water molecules that are between the hydrophobic and hydrophilic cases described above. To model these surfaces, we tune the polarity of the wall by rescaling the charges of the Si–O–H groups by a factor k, where $0 \leq k \leq 1$. When $k = 1$ the surface atoms retain their full charge listed in Table 1. When $k = 0$ the walls have no charge and the H atoms at the wall surface vanish from the potential because they lack any interaction with water molecules. A study of the contact angle of SPC/E water next to these walls by Giovambattista *et al.*[27] revealed that the walls are hydrophobic (contact angle greater than 90°) when $k \leq 0.4$ and hydrophilic (contact angle less than 90°) for values of $k > 0.4$.

Water molecules are confined to a small distance d in the z direction by placing two walls parallel to the xy plane and equidistant from the $z = 0$ plane. The cubic simulation box is periodic in all directions, but is chosen such that the walls span the simulation box in the x and y directions (*i.e.* the x and y dimensions of the walls and all sides of the cubic simulation box are 6.93 nm in length). Thus the SiO_2 lattice of the walls is uninterrupted in the x and y directions, and water is confined to a small distance d in the z direction. The separation distance between the walls, d, is defined to be the distance between the planes that contain the H atoms on the two walls. For the case when $k = 0$ and the H atoms vanish, the plane where the H atoms would lie is used (*i.e.* the position of the Si and O wall atoms is unchanged for all simulations with the same d). The confined volume is then defined to be the product of the square of the length of the simulation box times d; accordingly, the average mass density of the confined water, ρ, is the ratio of the mass of water molecules to the confined volume.

Table 1 Potential parameters for plate–water interactions (taken from ref. 81)

Atom	ε/kJ mol^{-1} [a]	σ/nm[a]	Charge/e[b]
O	0.6487	0.3154	−0.71
Si	0.5336	0.3795	0.31
H			0.40

[a] Lennard-Jones parameters for plate–water O atom interactions. [b] The full charges on Si–O–H groups ($k = 1$) at the surface of the walls. These point charges interact *via* Coulombic interactions with all the charges present on SPC/E water.

Confinement of a fluid by solid surfaces parallel to the xy plane results in inhomogeneities in the z direction. Consequently, the stress tensor for such materials is anisotropic, and two relevant pressures exist: a transverse pressure measured in the x and y directions ($P^{\parallel}$), and a normal pressure calculated in the z direction ($P^{\perp}$).[84] The virial expression was used to calculate the pressure parallel to the walls $P^{\parallel}$, accounting for the fixed locations of the atoms in the wall.[85] The pressure normal to the walls, $P^{\perp}$, was calculated by summing the total z projection of the force between water molecules and wall atoms, and then dividing by the surface area of the walls. For both pressures we adopt the convention that lateral and normal compression corresponds to positive stresses, and expansion in these directions corresponds to negative stresses.

To investigate the effects of wall–wall separation (d), density (ρ) and surface polarity (k), we studied 108 different sets of conditions that correspond to all combinations of: $d = 0.8$ and 1.6 nm, $k = 0$ to $k = 1$ in increments of 0.2, and $\rho = 0.4$ to 1.2 g cm^{-3} in increments of 0.1 g cm^{-3}. Constant NVT molecular dynamics simulations were used to generate equilibrium configurations of water confined at the above-listed conditions and $T = 300$ K. The rigid-body equations of motion were integrated using a half-step leap-frog Verlet scheme[86] for translation and an iterative quaternion algorithm[87] for rotation with a step size of $\delta t = 1$ fs. Each simulation was equilibrated at $T = 300$ K for 100 ps; 25 equilibrium configurations were then saved for each run at 5 ps intervals for use in generating ISs. The temperature was fixed for the entire simulation (*i.e.* equilibration and production) with a Berendsen thermostat.[88] Electrostatic interactions are treated using the Ewald sum technique with a cutoff of distance of 0.79 nm and parameters $m_{\max} = 5^3$ (for the number of vectors in the reciprocal space sum) and $\alpha = 4$ nm^{-1} (for the width of the screening-charge Gaussian distribution).[89,90] The linked-cell-list and neighbor-list methods[86,91] are employed to facilitate fast calculation of pair interactions.

The inherent structures (IS) were generated by minimizing the PE of an equilibrium configuration with respect to all degrees of freedom. Each water molecule has six degrees of freedom: the CM is specified with three Cartesian coordinates and the orientation is defined by three Euler angles.[92] An additional degree of freedom exists for each H atom on the walls (only present when $k > 0$, see above) because these atoms are permitted to reorient in a circle.† The PE hypersurface is then a function of $6N$ or $6N + N_H$ variables (N_H is the number of hydrogen atoms on the walls) when $k = 0$ and $k > 0$ respectively. The PE was minimized by performing a conjugate-gradient numerical approximation to steepest-descent energy minimization,[77,93] and the minimization was considered complete when the change in energy between two successive minimization steps was $\leq 10^{-15}$ kJ mol^{-1}. The three-dimensional analogue would correspond to the point on the PEL that represents the system moving downhill until it reaches a local minimum. The minima of the PEL satisfy

$$\nabla_{\boldsymbol{\Omega}} \Phi = 0$$

where Φ is the potential-energy surface and $\boldsymbol{\Omega}$ is the vector whose components are the degrees of freedom of the system (*i.e.* the CM positions and orientations of all water molecules and the angular coordinate of each H atom on the wall). The ISs are therefore mechanically stable arrangements of the molecules since the components of $\nabla_{\boldsymbol{\Omega}} \Phi$ are the net forces and torques on the molecules. This minimization was performed on all 25 equilibrium configurations produced at each set of conditions (*i.e.* set of k, ρ and d), allowing IS properties to be averaged over 25 different configurations.

† The hydrogen atoms move with fixed bond length and bond angle such that the position of each H atom can be specified with a single angle between 0 and 2π.

3 Results and discussion

Results are presented in two sections: section 3.1 addresses the mechanical properties of ISs; section 3.2 provides information on structural order present in ISs. All IS calculations are averages over 25 initial equilibrated configurations.

3.1 Mechanical properties

One approach to studying failure in glassy materials is to investigate mechanically stable configurations (*i.e.* ISs) under different states of strain. Such calculations provide insight into how glasses deform and fail. IS configurations can be collected at various macroscopic strain states by minimizing the potential energy of equilibrium configurations over a range of densities.‡ LaViolette and Stillinger first considered the relationship between the inherent structure pressure of bulk materials and density;[94] this relationship has since been termed the equation of state of an energy landscape (EOSEL).[95] In particular, a study by Sastry *et al.*[96] highlighted the fact that for atomic materials the pressure of ISs displays a minimum as a function of density. The density at which this minimum occurs is now referred to as the Sastry density, ρ_s. This corresponds to a state of maximum isotropic tensile stress, with the maximum isotropic tension given by $-P(\rho_s)$. IS configurations at ρ_s are at a state of maximum stress, and energy minimization at $\rho < \rho_s$ generates ISs that are in a state of strain beyond the point of mechanical failure. This causes the material to fissure and form voids that develop from "weak spots" present in the equilibrium configuration. Thus, ρ_s is the minimum density for which ISs are both mechanically stable and spatially homogeneous. Accordingly, ρ_s is an important material property, namely the lowest density at which a homogeneous glass can be formed. Subsequent studies have shown that these characteristics of the EOSEL are quite general, and apply also to molecular glasses.[97]

The investigation of Sastry *et al.* examined materials in bulk; using this energy minimization approach recent work has begun to explore, both theoretically[68,70] and computationally,[69] the properties of nanoscale films. One important difference with respect to bulk behavior is the anisotropy in the stress tensor caused by confinement (see section 2). Two relevant pressures exist, a normal pressure, $P^{\perp}$, and a transverse or parallel pressure, $P^{\parallel}$. Consequently there are two Sastry densities $\rho_s^{\parallel}$ and $\rho_s^{\perp}$. A numerical study by Shah and Truskett[69] examined LJ particles confined by structureless walls and found that these two densities and their associated maximum sustainable tensions $[-P^{\parallel}(\rho_s^{\parallel})$ and $-P^{\perp}(\rho_s^{\perp})]$ correspond to different modes of mechanical failure and directional material strengths. The direction with a larger value of ρ_s (*i.e.* maximum stress is reached at a smaller state of transverse strain) is more susceptible to failure. Additionally, voids were found to emerge at the larger of the two Sastry densities (*i.e.* at the smaller state of strain that corresponds to maximum stress). In this section we examine the corresponding behavior for water films confined by silica-based walls.

Fig. 1 shows the EOSEL, for $P^{\parallel}$ and $P^{\perp}$, at the two values of wall separation studied here ($d = 0.8$ and 1.6 nm) and over the full range of wall polarities ($0 \leq k \leq 1$). Thin films exhibit complex behavior, especially under hydrophobic confinement ($k \leq 0.4$). In this case, the transverse stress (Fig. 1a) exhibits both a high-density extremum at 1.1 g cm^{-3} and an inflection point with almost vanishing slope at 0.8 g cm^{-3}. The normal stress (Fig. 1b) displays a single extremum across the entire polarity range, although inflections at high density become evident for $k \leq 0.4$. For $k \geq 0.8$, corresponding to strong water–wall interactions, the transverse and normal directions have single minima between $\rho = 0.8$ and 0.9 g cm^{-3}. Thick

‡ Decreasing density at fixed separation distance corresponds to increasing the transverse strain.

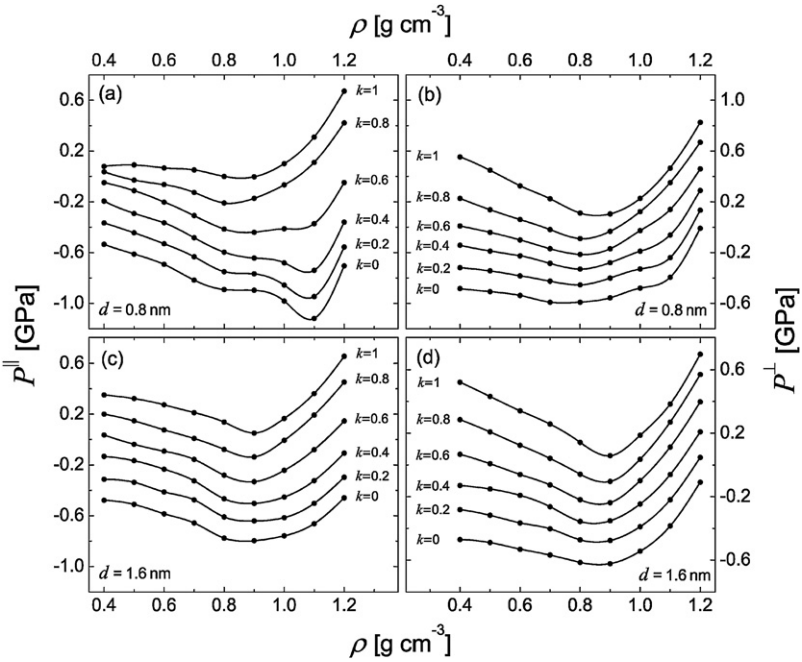

Fig. 1 Equation of state of the energy landscape (pressure as a function of density for inherent structures) of water under various confinement conditions: (a) $P^{\parallel}$ for $d = 0.8$ nm, (b) $P^{\perp}$ for $d = 0.8$ nm, (c) $P^{\parallel}$ for $d = 1.6$ nm, and (d) $P^{\perp}$ for $d = 1.6$ nm. Each plot shows all six studied values of k with the curves shifted vertically for clarity. The values of k for all plots from the bottom to top are $k = 0$ [−0.4 GPa], $k = 0.2$ [−0.2 GPa], $k = 0.4$, $k = 0.6$ [+0.2 GPa], $k = 0.8$ [+0.4 GPa], $k = 1$ [+0.6 GPa]. The standard deviation among the computed pressures, calculated across 25 inherent structures for each data point, is smaller than the size of the data symbols.

films ($d = 1.6$ nm) display a single minimum at $\rho = 0.9$ g cm^{-3} in the EOSEL in the transverse and normal directions.

In analogy with bulk behavior, the single minima shown in Fig. 1c and d for thick films correspond to mechanical stability limits, with progressively larger voids appearing as the limiting strain is exceeded (*i.e.* the Sastry density is at the minimum of the EOSEL). In contrast, the high-density extremum in the transverse stress for thin films at $\rho = 1.1$ g cm^{-3}, seen for films confined by non-polar and weakly polar walls ($k \leq 0.4$), corresponds to strain-induced disruption of a highly structured trilayer film whose two outer layers exhibit long-range crystalline order. Voids emerge in these films between $\rho = 0.8$ and 0.9 g cm^{-3}. Thus the high-density minimum is not associated with loss of mechanical stability, and the Sastry density for these films corresponds to the low-density inflection point in Fig. 1a for $k \leq 0.4$. This will be discussed in detail in section 3.2.1, where the structure of the films is analyzed. It then follows that for all films, $\rho_s^{\parallel}$ and $\rho_s^{\perp}$ lie between 0.8 and 0.9 g cm^{-3} for the transverse and normal directions.§ This is the density range where loss of mechanical stability occurs.

The effect of wall polarity (k) and film thickness (d) on the mechanical strength of thin water films can be determined by comparing the maximum tension for each value of k and d. Fig. 2 plots the tension ($-P^{\parallel}$ and $-P^{\perp}$) of IS configurations at the minimum of the EOSEL in Fig. 1. For thick films ($d = 1.6$ nm) the maximum

§ In this work, the strain resolution is 0.1 g cm^{-3}. Differences between $\rho_s^{\parallel}$ and $\rho_s^{\perp}$ cannot be determined more precisely; additional simulations would be required for this.

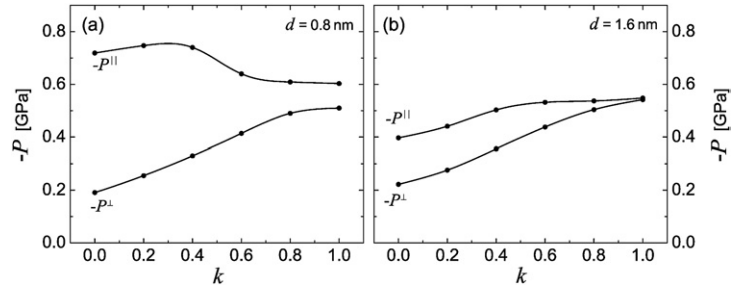

Fig. 2 Maximum sustainable tension for the transverse and normal directions as a function of wall polarity k for separations of (a) $d = 0.8$ nm and (b) $d = 1.6$ nm. These points correspond to the minimum pressure values of the curves in Fig. 1. The standard deviation among the computed pressures, calculated across 25 inherent structures for each data point, is smaller than the size of the data symbols.

tension increases with k in both the transverse and normal directions; the film can withstand more stress as the interaction strength between water and the wall is increased. This trend is also valid for thin films ($d = 0.8$ nm) in the normal direction, but not in the transverse direction. Fig. 2a shows that the maximum lateral stress increases with k in the hydrophobic regime ($k \leq 0.4$), but decreases with k in the hydrophilic region ($k \geq 0.6$). Understanding this behavior requires examination of the structure of confined water near hydrophobic surfaces. This will be addressed in section 3.2.1. A notable feature of Fig. 2 is the strong correlation between substrate hydrophobicity and stress anisotropy. Under hydrophobic confinement, water films are much stronger in the transverse than in the normal direction. However, for hydrophilic confinement $-P^{\parallel}$ and $-P^{\perp}$ are considerably closer.

Minimizing the potential energy of confined water at low density results in the formation of ISs that contain voids. We define the void space to be the volume comprising all points that lie a distance of more than 0.316 nm (the LJ σ value for SPC/E water) from any O atom belonging to a water molecule or the wall. The location of these voids provides information about the failure mechanism. Void probability profiles were determined by performing 10^6 trial point insertions in a slice of thickness $\delta z = 0.02$ nm. The ratio of successful insertions (point belongs to void space) to total insertions is the void probability within that slice. Fig. 3 shows the void probability profiles in thin ($d = 0.8$ nm) glassy films for the hydrophobic ($k = 0$) and the hydrophilic ($k = 1$) walls, and for densities $0.4 \leq \rho \leq 0.9$ g cm^{-3}.

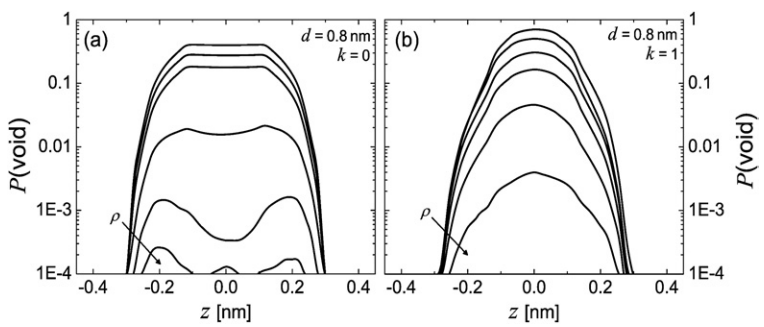

Fig. 3 Probability of finding a void in the water film for walls where (a) $k = 0$, and (b) $k = 1$. Both are for a separation of $d = 0.8$ nm with the middle of the film at $z = 0$ and the wall surfaces at $|z| = 0.4$ nm. Density increases from 0.4 g cm^{-3} to 0.9 g cm^{-3} in intervals of 0.1 g cm^{-3} as indicated by arrows. The profiles are similar for $d = 1.6$ nm.

At $\rho \geq 1.0$ g cm^{-3} the void probability is negligible. Therefore, the values of $\rho_s^{\parallel}$ and $\rho_s^{\perp}$ discussed above are consistent with the density at which voids emerge. In addition, the z position where voids are most likely to form is strongly dependent on the polarity of the confining surfaces. For $k = 0$, the void profile at $\rho = 0.7$, 0.8 and 0.9 g cm^{-3} develops maxima near the walls; when $k = 1$, the profile has a single peak in the middle of the film. These void profiles are characteristic of the other values of k [*i.e.* when $k \leq 0.4$ ($k \geq 0.6$) the void profiles have the same general shape as the $k = 0$ ($k = 1$) case].

Fig. 4 shows two examples of voids present in the ISs of water at $\rho < \rho_s$, when confined by hydrophobic (Fig. 4a) and hydrophilic (Fig. 4b) surfaces. These pictures are consistent with the void profiles seen in Fig. 3. The void that forms in water under hydrophobic confinement is near the wall, while hydrophilic confinement leads to mechanical failure in the middle of the film. The difference in void location can be understood by comparing the self-interaction of water with the strength of its interaction with the wall when $k = 0$ and $k = 1$. Fig. 5 displays the profile of the potential energy per water molecule under hydrophobic ($k = 0$) and hydrophilic ($k = 1$) confinement. In Fig. 5a and b the potential energy is split into water–water and water–wall contributions. Fig. 5c shows the total potential energy per water molecule for $k = 0$ and $k = 1$; this is the sum of the curves in Fig. 5a and b. Under hydrophobic confinement with $k = 0$, only dispersive interactions exist between water and the wall, and Fig. 5a shows that the water–water interaction energy is much stronger than the water–wall energy, even close to the confining surface. This is due to the strong electrostatic interactions between water molecules. This results in "weak spots" near the walls that, at $\rho < \rho_s$, develop into voids upon energy minimization. The detachment of water molecules from the wall is indicative of adhesive failure. Under hydrophilic confinement, Fig. 5b shows that the attractive energy for water–wall interactions is stronger than that for water–water interactions when $|z| \geq 0.7$ nm. Thus near the confining surface, the interaction between water and the wall is stronger than that between water molecules. This causes the formation of voids in the middle of the film and leads to cohesive failure at $\rho < \rho_s$.

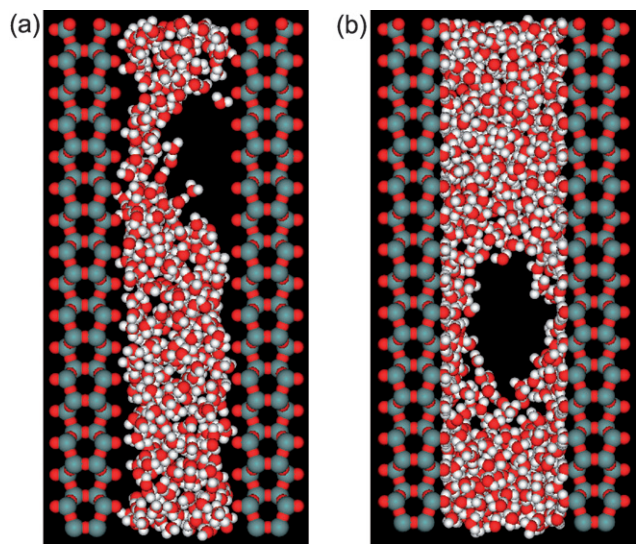

Fig. 4 Voids present in ISs of water confined between (a) hydrophobic surfaces with $k = 0$, and (b) hydrophilic walls with $k = 1$. Both are IS configurations at $\rho = 0.8$ g cm^{-3} with a separation of $d = 1.6$ nm. Water molecules have been removed for ease of visualization from the front and rear of the void (*i.e.* the voids do not pass through the entire simulation box). Si, O and H atoms are represented by gray, red and white spheres respectively.

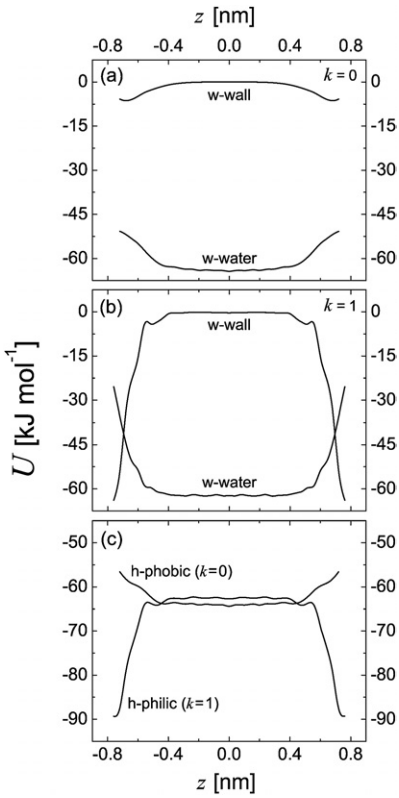

Fig. 5 Potential-energy profiles of water molecules under hydrophobic confinement with $k = 0$ (a) and hydrophilic confinement with $k = 1$ (b) at $\rho = 0.8$ g cm^{-3} and $d = 1.6$ nm (the same conditions as in Fig. 4). Energies shown are on a per water molecule basis, and the potential energy is split into water–water (w-water) and water–wall (w-wall) contributions. (c) The total potential energy per water molecule (water–water and water–wall contributions) for hydrophobic and hydrophilic confinement at the same conditions as in (a) and (b) respectively.

3.2 Structure

Inherent structures formed from equilibrium liquid configurations are amorphous and lack long-range order; hence these configurations are representative of glasses. However, the atomic structure of the silica walls and the interactions between water molecules and the walls impose two distinct types of order. One type is evident at high density near hydrophobic walls and the other is present at low density alongside hydrophilic walls. Accordingly, section 3.2.1 examines ISs for $k = 0$, $d = 0.8$ nm and $\rho = 1.2$ g cm^{-3}, and section 3.2.2 analyzes IS configurations with $k = 1$, $d = 0.8$ nm and $\rho = 0.4$ g cm^{-3}.

3.2.1 Hydrophobic Confinement. Confinement negates the structural isotropy characteristic of bulk liquids. One approach to studying the structure of confined materials is to examine the local density along the direction of confinement. A density profile along the z direction is calculated by assigning water molecules to 0.02 nm thick bins in the z direction, according to the position of the O atom. The density in each bin is computed from the total mass of water molecules in the slab, divided by its volume. The density profiles for $k = 0$ and $d = 0.8$ nm are shown in Fig. 6 for the entire range of studied mean densities. Fig. 6a shows a bilayer structure that is present at average densities up to $\rho = 0.8$ g cm^{-3}. At $\rho \geq 0.9$ g cm^{-3} a third

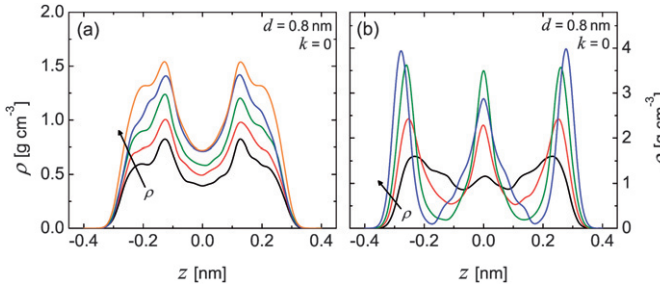

Fig. 6 Density profiles for water confined between hydrophobic walls with $k = 0$ and $d = 0.8$ nm. The wall surfaces are located at $|z| = 0.4$ nm. (a) The underlying structure is bilayer when $\rho \leq 0.8$ g cm^{-3}, and (b) trilayer when $\rho \geq 0.9$ g cm^{-3}. On plot (a) the average densities are $\rho = 0.4$ g cm^{-3} (black), $\rho = 0.5$ g cm^{-3} (red), $\rho = 0.6$ g cm^{-3} (green), $\rho = 0.7$ g cm^{-3} (blue) and $\rho = 0.8$ g cm^{-3} (orange). On plot (b) the average densities are $\rho = 0.9$ g cm^{-3} (black), $\rho = 1.0$ g cm^{-3} (red), $\rho = 1.1$ g cm^{-3} (green) and $\rho = 1.2$ g cm^{-3} (blue). Arrows indicate the direction of increasing density.

layer of water molecules develops as seen in Fig. 6b. The density range over which this transition occurs coincides with the inflection point (*i.e.* the Sastry density) in the EOSEL for thin films confined by hydrophobic walls (Fig. 1a). The bilayer-to-trilayer transition occurs for $d = 0.8$ nm when $k \leq 0.6$. For thicker films ($d = 1.6$ nm), six layers of water are present at high density for all values of k and there is no clear layering transition.

Examining configurations of water molecules that belong to a single peak in the density profile provides detailed structural information. Fig. 7 shows a characteristic arrangement of water molecules that constitute one of the two symmetric outer peaks (*i.e.* the O atom of the water molecule is located at $|z| > 0.18$ nm) of the density profile for $\rho = 1.2$ g cm^{-3}. This monolayer of water molecules is approximately 0.2 nm thick and self-assembles into a hexagonal lattice. The same structure is evident in the first layer of water molecules next to the wall when $\rho \geq 1.0$ g cm^{-3} and $k \leq 0.6$ for $d = 0.8$ and 1.6 nm. The hexagonal order becomes less pronounced as the density decreases and k increases.

In the perfect lattice, water molecules can adopt two configurations: (i) with a single H atom pointing away from the wall and (ii) with both H atoms in a plane nearly parallel to the surface. These configurations alternate, and water molecules form six-membered rings, giving rise to a hexagonal lattice. Thus each water molecule participates in four hydrogen bonds (HB): three of these point roughly parallel to the wall and correspond to HBs with water molecules in the same layer, and one

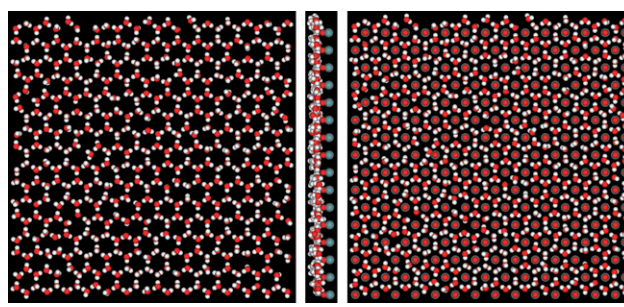

Fig. 7 Inherent structure configuration showing water molecules within 0.22 nm of a hydrophobic wall with $k = 0$, $\rho = 1.2$ g cm^{-3} and $d = 0.8$ nm (left); profile view of the same layer with surface wall atoms included (middle); with surface Si and O wall atoms included (right). Si, O and H atoms are represented by gray, red and white spheres respectively.

points normal to the substrate surface and corresponds to a HB with a water molecule in the adjacent layer. The structure in Fig. 7 has defects that can be attributed to the presence of a middle layer of water molecules that is disordered.

Closer inspection of the monolayer in Fig. 7 reveals that the center of each hexagonal ring of water molecules is occupied by an oxygen atom on the surface of the wall. This strict correlation between the substrate and water suggests that the lattice is templated by the wall. At high density, water molecules are pushed into the small spaces between the top layer of Si and O atoms on the substrate surface. These water molecules self-assemble into a hexagonal lattice in order to participate in four HBs. Thus it is the atomic structure of the wall that imposes the hexagonal lattice on the water. This conclusion is supported by the amorphous character of the middle peak (or peaks when $d = 1.6$ nm) of the density profile. Without the hexagonal template provided by the wall, no long-range order exists for water molecules in the middle of the film.

This structure has been previously observed[82] for SPC/E water confined by identical silica walls at a separation of $d = 0.6$ nm and $T = 300$ K. At this value of d only two layers of water are present, and in the bilayer ice these layers are in registry. It was found that the crystal structure was very sensitive to the value of d and this hexagonal lattice was not evident at $T = 300$ K in simulations with $d = 0.8$ or 1.6 nm. Those simulations were done at constant pressure and examined confined water that was in contact with a bulk water reservoir.[82] The highest densities studied were approximately 1.0 g cm^{-3}, which is the lowest density at which the hexagonal lattice is evident in the IS configurations.

It is now appropriate to resume the discussion of the EOSEL for $P^{\|}$ at $d = 0.8$ nm (see Fig. 1a and 2a) and examine why the minimum of the EOSEL does not correspond to the emergence of voids at $k \leq 0.4$ and $d = 0.8$ nm. Under hydrophobic confinement with $k = 0$ there is a sharp minimum in $P^{\|}$ at $\rho = 1.1$ g cm^{-3}; as k increases this minimum becomes less prominent. At $k = 0.6$, only a shoulder in the EOSEL is present at $\rho = 1.1$ g cm^{-3}, and at $k \geq 0.8$ the feature has completely receded. This behavior is caused by the hexagonal ordering of water molecules near the wall at these conditions. The ordered arrangement of water at both walls increases the strength of the thin film, resulting in a deep minimum in $P^{\|}$ at $\rho = 1.1$ g cm^{-3}. Thus, for $k \leq 0.4$ at a separation $d = 0.8$ nm, the minimum of the EOSEL does not correspond to the emergence of voids in system, but represents the density below which the arrangement of water next to the wall begins to disorder. Accordingly, for these conditions $-P^{\|}$ at the minimum represents the maximum stress that the film can withstand before significant defects become present in the lattice near the wall.

This observation raises the question of why similar behavior is not evident for thick films ($d = 1.6$ nm). The answer lies in the limited ability of the wall to impose order beyond the first layer of water molecules. The hexagonal template of the walls results in the ordering of a single layer of water next to the surface. At $d = 0.8$ nm this means that the two outer layers are organized into hexagonal lattices and the one middle layer is amorphous. However, at $d = 1.6$ nm there are four amorphous inner layers and two ordered outer layers. The trilayer thin film ($d = 0.8$ nm) is thus much stronger than its six-layer thicker counterpart ($d = 1.6$ nm): the maximum sustainable tension for $d = 0.8$ nm is more than 300 MPa greater than for $d = 1.6$ nm.

3.2.2 Hydrophilic confinement. Structural ordering of water molecules is also evident near hydrophilic surfaces. Examination of the density profiles in Fig. 8a for $k = 1$, $d = 0.8$ nm and $0.4 \leq \rho \leq 0.8$ g cm^{-3} reveals two sharp outer peaks next to the confining surfaces. The first peak (located closest to the confining walls) corresponds to $0.36 < |z| < 0.4$ nm. The second peak is slightly closer to the middle of the film and corresponds to $0.28 < |z| < 0.36$ nm. At $\rho = 0.4$ g cm^{-3} the outer peak is significantly higher than the inner peak. However, as the average density increases from $\rho = 0.4$ to 0.8 g cm^{-3}, the outer peak recedes and the inner peaks grows.

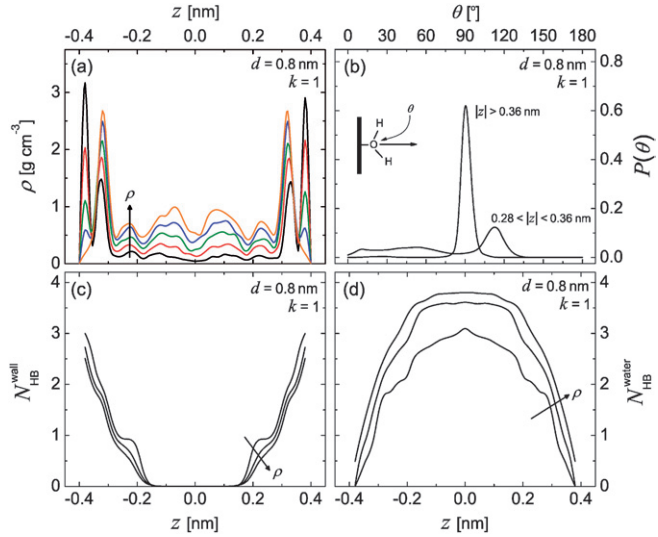

Fig. 8 (a) Density profiles for water confined between hydrophilic walls with $k = 1$ and $d = 0.8$ nm for low density, $\rho \leq 0.8$ g cm^{-3}. The wall surfaces are located at $|z| = 0.4$ nm. The average densities are $\rho = 0.4$ g cm^{-3} (black), $\rho = 0.5$ g cm^{-3} (red), $\rho = 0.6$ g cm^{-3} (green), $\rho = 0.7$ g cm^{-3} (blue) and $\rho = 0.8$ g cm^{-3} (orange). Arrow indicates the direction of increasing density. (b) Probability distribution of the angle formed between the O–H bond of a water molecule and a vector normal to the wall that points into the water film. The two curves are $P(\theta)$ for molecules in the outer peak of the density profile with $|z| > 0.36$ nm, and the inner peak with $0.28 < |z| < 0.36$ nm. (c) Average number of HBs per water molecule formed between water and wall atoms with confining surfaces located at $|z| = 0.4$ nm. (d) Average number of HBs per water molecule formed with other water molecules. In (c) and (d) the densities are $\rho = 0.4$, 0.8 and 1.2 g cm^{-3}. Arrows indicate the direction of increasing density.

Once $\rho \geq 0.8$ g cm^{-3}, the outer peak no longer exists and the inner peak corresponds to a local density over 2.5 g cm^{-3}. Since each peak corresponds to a layer of water molecules, this behavior indicates a significant change in the layering of water near the walls as a function of mean density. It is important to note that simulations at $T = 300$ K have shown the stability limit of liquid water confined by hydrophilic plates ($k = 1$) to be approximately 0.7 g cm^{-3} for all values of d.[82] Thus the IS configurations that result in the behavior evident in Fig. 8 are calculated from an inhomogeneous phase-separated system.

To probe the structure of water molecules near the confining surface we focus on their orientation, and in particular the angle θ formed by an O–H bond of a water molecule and a vector normal to the wall surface pointing into the film (see diagram in Fig. 8b). Fig. 8b shows the probability distribution of θ for water molecules located at $|z| > 0.36$ nm and $0.28 < |z| < 0.36$ nm (the outer and inner peaks of the density profile respectively) for $0.4 \leq \rho \leq 0.8$ g cm^{-3}. $P(\theta)$ shows a single maximum at $\theta = 90°$ for molecules that constitute the outer peak. This indicates that water molecules closest to the wall ($|z| > 0.36$ nm) are oriented parallel to the substrate surface and lie in the xy plane. $P(\theta)$ for molecules in the inner peak of the density profile ($0.28 < |z| < 0.36$ nm) has a small maximum near the tetrahedral angle ($\theta = 109°$); molecules in this region show comparatively less orientational preference.

Under hydrophilic confinement, water is capable of forming HBs with the charged Si–O–H groups on the substrate surface, as well as with other water molecules. Fig. 8c shows the average number of HBs (per water molecule) that are formed between a water molecule and the wall as a function of z; Fig. 8d shows the corresponding average number of water–water HBs per molecule. Hydrogen bonds are defined by standard geometric criteria that specify distance and angle

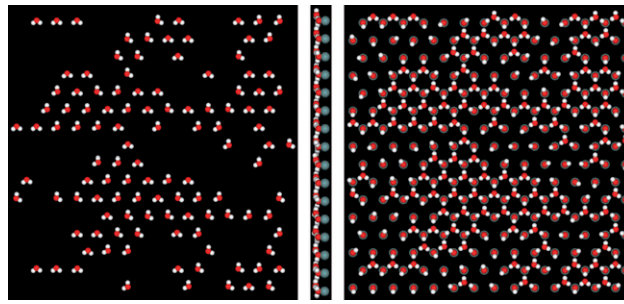

Fig. 9 Inherent structure configuration showing water molecules within 0.04 nm of a hydrophilic wall with $k = 0$, $\rho = 0.4$ g cm^{-3} and $d = 0.8$ nm (left); profile view of the same layer with surface wall atoms included (middle); with surface Si, O and H wall atoms included (right). Si, O and H atoms are represented by gray, red and white spheres respectively.

requirements [98] and we count the number of HBs that each water molecule participates in (*i.e.* coordination number). These plots indicate that water molecules close to the hydrophilic wall ($|z| > 0.36$ nm) form on average three HBs with Si–O–H groups at the surface, and less than one HB with other water molecules. Also, as the density increases, the average number of HBs between water and the wall decreases, and the average number of water–water HBs increases.

Fig. 9 shows a representative configuration of water molecules that constitute the outer peak of the density profile, $0.36 < |z| < 0.4$ nm for $\rho = 0.4$ g cm^{-3}. In this layer each water molecule is oriented parallel to the xy plane, in agreement with $P(\theta)$ in Fig. 8b. Furthermore, if this configuration is placed on top of the Si–O–H groups that compose the surface of each wall, it is clear that the water molecules and the charged H atoms on the wall surface are arranged such that three HBs are formed between each water molecule and the wall.¶ This is consistent with Fig. 8c which shows that when $\rho < 0.8$ g cm^{-3}, water molecules located at $0.36 > |z| > 0.4$ nm form three HBs with the wall. A similar inspection of the configuration of water molecules in the second peak ($0.28 > |z| > 0.36$ nm) reveals that this layer lacks long-range order at all studied densities. Fig. 8c and d show that water molecules in this layer form on average one less HB with the wall and one more HB with other water molecules. Thus, the loss of one HB with the wall is enough to prevent structural order near hydrophilic walls. Very similar behavior of the density profiles in Fig. 8a and the structure in Fig. 9 is evident when the separation is increased to $d = 1.6$ nm (Figures not shown).

The structure apparent in Fig. 9 results from the ability of water molecules to participate in four HBs. At low density ($\rho = 0.4$ g cm^{-3}), this propensity for hydrogen bonding is satisfied by forming in-plane bonds with the wall as explained above. Furthermore, under these conditions there is very little water in the region between the confining surfaces [*e.g.* $|z| < 0.3$ nm; see Fig. 8a], and hence hydrogen bonding between water molecules close to the surface and those between the confining surfaces is minimal. Thus, the arrangement of water molecules in Fig. 9 results from three features of the confining walls: (i) the strong electrostatic interactions of charged Si–O–H groups with water molecules, (ii) cavities on the structured silica surface that can accommodate one water molecule, and (iii) the ability of hydrogen atoms on the silica surface to reorient with fixed bond length and bond angle. This reasoning also explains why the outside peak of the density profile decreases with density. At higher densities, the abundance of water molecules creates a competition for HBs between neighboring water molecules and the surface. Hence,

¶ During energy minimization the position of each H atom on the wall surface is optimized in addition to the position and orientation of each water molecule (see section 2).

on average, water molecules form fewer HBs with the surface and more with other water molecules as density increases (see Fig. 8c and d). This prevents the arrangement seen in Fig. 9 from occurring.

4 Conclusions

In this work, we have used molecular simulations and the PEL paradigm to explore the structure and mechanical properties of thin glassy-water films confined between atomically detailed, silica-based surfaces with continuously tunable hydrophobicity and hydrophilicity. The mechanical properties of water films were explored by calculating how the state of strain affects mechanically stable configurations. Loss of mechanical stability occurs between 0.8 and 0.9 g cm^{-3} for all values of wall polarity (k) and separation (d). Below such densities, progressively larger fissures appear and mechanically stable configurations are no longer homogeneous. Thus the Sastry density (ρ_s) was determined to be in the 0.8–0.9 g cm^{-3} range for all polarities and separations investigated. In the bulk, ρ_s corresponds to the minimum in the EOSEL; our results in confinement are consistent with this except for thin films ($d = 0.8$ nm) bounded by hydrophobic ($k \leq 0.4$) walls. Under these conditions, ρ_s corresponds to a low-density inflection point in the EOSEL, and the high-density minimum in the stress–strain curve corresponds to the disruption of a hexagonal lattice of water molecules in the two outer layers of a trilayer film. This specific structure also results in a substantial stress anisotropy for confined water. The maximum transverse stress is much larger than the normal stress for water confined by hydrophobic surfaces. In contrast, water confined by hydrophilic surfaces shows closer values for the maximum normal and transverse stress. Additionally, the substrate–water interactions were observed to have a strong influence on the mode of mechanical failure. For values of $k \leq 0.4$ (hydrophobic) the film failed adhesively, with the development of voids next to the confining surface. For $k \geq 0.6$ (hydrophilic) voids form in the middle of the film, leading to cohesive failure.

A salient result of this study is the ability of the confining surfaces to impose long-range structural order on the first layer of water molecules next to the wall. A hexagonal lattice is evident at high density under hydrophobic confinement. At $\rho \geq 1.0$ g cm^{-3}, water molecules are forced close to the wall and into the small cavities between the substrate surface atoms. The architecture of these cavities is such that water molecules adopt one of two alternating orientations in an attempt to participate in four HBs. The result is a hexagonal lattice of water molecules in which the center of each hexagon is occupied by a surface oxygen atom. Under hydrophilic confinement and low density, water molecules position themselves to form three HBs with Si–O–H groups on the surface. It is the strong electrostatic interactions between water and the charged surface groups and the ability of H atoms on the surface to reorient that cause this behavior. In both of these cases the hydrophobic and hydrophilic walls template an ordered monolayer and submonolayer of water molecules respectively; the atomic details and different interactions permit the formation of these complex structures. The ability of ordered surfaces to template structured water configurations, and the profound influence that such configurations impart to the entire film suggests that smooth walls, though frequently used in simulations, may not be able to capture an important range of properties and phenomena associated with thin films of molecular glasses.

Glasses are nonequilibrium materials, hence their properties are history-dependent, and differences in the formation process lead to materials with distinct characteristics. This study examined glassy configurations formed *via* energy minimization, a process akin to quenching a liquid instantaneously. Experimentally, however, glasses are formed by cooling a liquid at a finite rate that is sufficiently fast to avoid crystallization. A complementary study in which confined liquid configurations are cooled at various finite rates into the glassy state is in progress and will be the subject of a future publication.

The large number of factors affecting confined materials leaves much room for future work. This study demonstrated the strong influence of confining surfaces on water; in particular, the architecture and interactions of the confining substrate are capable of inducing long-range order in the first layer of water close to the substrate. These structures were found to have important consequences for the mechanical properties of thin water films, especially for hydrophobic confinement. Future studies should address how features such as surface curvature and heterogeneity affect the properties and structure of confined glassy water. The surfaces used in this study can easily be modified to include various patterns or patches of hydrophobicity/hydrophilicity. Alternatively, an entirely different confining surface such as a protein,[67] can be studied to provide results that are relevant to biotechnology and the preservation of labile biomolecules in the glassy state. Improved knowledge of these topics would represent a significant advance in the quest for a deeper molecular-based understanding of nano-confined materials and their applications.

Acknowledgements

We thank F. H. Stillinger for fruitful discussions. P. G. D. gratefully acknowledges the financial support of the National Science Foundation Collaborative Research in Chemistry Grant No. CHE0404699, and of Unilever Research U. S.

References

1 D. Eisenberg and W. Kauzmann, *Structure and Properties of Water*, Oxford University Press, New York, USA, 1969.
2 F. Franks, *Water: a Matrix of Life*, The Royal Society of Chemistry, Cambridge, UK, 2nd edn, 2000.
3 P. Ball, *Life's Matrix: A Biography of Water*, University of California Press, California, 2001.
4 C. Tanford, *The Hydrophobic Effect: Formation of Micelles and Biological Membranes*, Wiley, New York, 2nd edn, 1980.
5 W. Kauzmann, *Adv. Protein Chem.*, 1959, **14**, 1.
6 J. M. Orten and O. W. Neuhaus, *Human Biochemistry*, Mosby, St. Louis, 10th edn, 1982.
7 Y. Levy and J. N. Onuchic, *Annu. Rev. Biophys. Biomol. Struct.*, 2006, **35**, 389.
8 P. G. Debenedetti and H. E. Stanley, *Phys. Today*, 2003, **56**, 40.
9 C. A. Angell, *Annu. Rev. Phys. Chem.*, 1983, **34**, 593.
10 P. G. Debenedetti, *J. Phys.: Condens. Matter*, 2003, **15**, R1669.
11 H. Kanno and C. A. Angell, *J. Chem. Phys.*, 1979, **70**, 4008.
12 K. T. Gillen, D. C. Douglass and J. R. Hoch, *J. Chem. Phys.*, 1972, **57**, 5117.
13 P. H. Poole, F. Sciortino, U. Essmann and H. E. Stanley, *Nature*, 1992, **360**, 324.
14 O. Mishima, L. D. Calvert and E. Whalley, *Nature*, 1985, **314**, 76.
15 T. Loerting, C. Salzmann, I. Kohl, E. Mayer and A. Hallbrucker, *Phys. Chem. Chem. Phys.*, 2001, **3**, 5355.
16 T. Loerting and N. Giovambattista, *J. Phys.: Condens. Matter*, 2006, **18**, R919.
17 C. A. Angell, *Science*, 2008, **319**, 582.
18 R. M. Barrer, *Zeolites and Clay Minerals As Sorbents and Molecular Sieves*, Academic Press, London, 1978.
19 E. Roedder, *Rev. Mineral.*, 1984, **12**, 1.
20 Special issue 'Lab on a Chip': Nature, 2006, **442**, 367.
21 Y. Gogotsi, N. Naguib and J. A. Libera, *Chem. Phys. Lett.*, 2002, **365**, 354.
22 B. J. Fuller, N. Lane, and E. E. Benson, *Life in the Frozen State*, CRC Press, Boca Raton, Florida, 2004.
23 P. Mentre, *Cell. Mol. Biol.*, 2001, **47**, 709.
24 V. Helms, *ChemPhysChem*, 2007, **8**, 23.
25 J. Dzubiella, J. M. J. Swanson and J. A. McCammon, *Phys. Rev. Lett.*, 2006, **96**, 087802.
26 F. Bresme and A. Wynveen, *J. Chem. Phys.*, 2007, **126**, 044501.
27 N. Giovambattista, P. G. Debenedetti and P. J. Rossky, *J. Phys. Chem. B*, 2007, **111**, 9581.
28 N. Giovambattista, P. G. Debenedetti and P. J. Rossky, *J. Phys. Chem. C*, 2007, **111**, 1323.
29 L. Hua, X. H. Huang, P. Liu, R. H. Zhou and B. J. Berne, *J. Phys. Chem. B*, 2007, **111**, 9069.
30 Y. K. Cheng and P. J. Rossky, *Nature*, 1998, **392**, 696.

31 F. Mallamace, M. Broccio, C. Corsaro, A. Faraone, D. Majolino, V. Venuti, L. Liu, C. Y. Mou and S. H. Chen, *Proc. Natl. Acad. Sci. U. S. A.*, 2007, **104**, 424.
32 L. Liu, S. H. Chen, A. Faraone, C. W. Yen and C. Y. Mou, *Phys. Rev. Lett.*, 2005, **95**, 117802.
33 J. Swenson, *Phys. Rev. Lett.*, 2006, **97**, 189801.
34 S. Cerveny, J. Colmenero and A. Alegría, *Phys. Rev. Lett.*, 2006, **97**, 189802.
35 S. H. Chen, L. Liu and A. Faraone, *Phys. Rev. Lett.*, 2006, **97**, 189803.
36 S. Yoshioka and Y. Aso, *J. Pharm. Sci.*, 2007, **96**, 960.
37 W. Wang, *Int. J. Pharm.*, 2000, **203**, 1.
38 J. Lee and S. Timasheff, *Biochemistry*, 1974, **13**, 257.
39 R. Hatley, F. Franks and S. Mathias, *Process Biochem.*, 1987, **22**, 169.
40 T. A. Jennings, *Lyophilization: Introduction and Basic Principles*, Interpharm Press, Englewood, CO, 1999.
41 C. J. Roberts and P. G. Debenedetti, *AIChE J.*, 2002, **48**, 1140.
42 S. D. Allison, M. C. Manning, T. W. Randolph, K. Middleton, A. Davis and J. F. Carpenter, *J. Pharm. Sci.*, 2000, **89**, 199.
43 W. Garzon-Rodriguez, R. L. Koval, S. Chongprasert, S. Krishnan, T. W. Randolph, N. W. Warne and J. F. Carpenter, *J. Pharm. Sci.*, 2004, **93**, 684.
44 D. Q. M. Craig, P. G. Royall, V. L. Kett and M. L. Hopton, *Int. J. Pharm.*, 1999, **179**, 179.
45 M. Pikal, Freeze-Drying/Lyophilization of Pharmaceutical and Biological Products, in *Drugs and the Pharmaceutical Sciences*, ed. L. Rey and J. May, Informa Health Care, U. S. A., 2004, p. 63.
46 S. Shamblin, in *Lyophilization of Biopharmaceuticals (Biotechnology: Pharmaceutical Aspects)*, ed. H. Constantino and M. Pikal, American Association of Pharmaceuticals, Arlington, VA, 2004, p. 229.
47 C. A. Oksanen and G. Zografi, *Pharm. Res.*, 1990, **7**, 654.
48 C. Ahlneck and G. Zografi, *Int. J. Pharm.*, 1990, **62**, 87.
49 B. C. Hancock and G. Zografi, *Pharm. Res.*, 1994, **11**, 471.
50 Y. H. Lam, R. Bustami, T. Phan, H. K. Chan and F. Separovic, *J. Pharm. Sci.*, 2002, **91**, 943.
51 V. Molinero and W. A. Goddard, *Phys. Rev. Lett.*, 2005, **95**, 045701.
52 J. Carpenter, B. Chang, and T. Randolph, in *Lyophilization of Biopharmaceuticals (Biotechnology: Pharmaceutical Aspects)*, ed. H. Constantino and M. Pikal, American Association of Pharmaceuticals, Arlington, VA, 2004, p. 423.
53 S. Yoshioka, Y. Aso and S. Kojima, *Pharm. Res.*, 2001, **18**, 256.
54 F. Franks, *Biophysics and Biochemistry at Low Temperatures*, Cambridge University Press, Cambridge, UK, 1985.
55 K. Storey and J. Storey, in *Insects at Low Temperature*, ed. R. E. Lee and D. L. Denlinger, Chapman and Hall, New York, 1991.
56 A. L. Devries, *Annu. Rev. Physiol.*, 1983, **45**, 245.
57 J. Duman, L. Xu, L. Neven, D. Tursman, and D. Wu, in *Insects at Low Temperature*, ed. R. E. Lee and D. L. Denlinger, Chapman and Hall, New York, 1991.
58 P. L. Privalov, *Crit. Rev. Biochem. Mol. Biol.*, 1990, **25**, 281.
59 M. S. Pometun, R. W. Peterson, C. R. Babu and A. J. Wand, *J. Am. Chem. Soc.*, 2006, **128**, 10652.
60 D. Paschek, S. Nonn and A. Geiger, *Phys. Chem. Chem. Phys.*, 2005, **7**, 2780.
61 P. G. Debenedetti, *Metastable Liquids: Concepts and Principles*, Princeton University Press, Princeton, NJ, 1996.
62 R. S. Smith, T. Zubkov and B. D. Kay, *J. Chem. Phys.*, 2006, **124**, 114710.
63 R. S. Smith and B. D. Kay, *Nature*, 1999, **398**, 788.
64 S. M. McClure, D. J. Safarik, T. M. Truskett and C. B. Mullins, *J. Phys. Chem. B*, 2006, **110**, 11033.
65 S. M. McClure, E. T. Barlow, M. C. Akin, D. J. Safarik, T. M. Truskett and C. B. Mullins, *J. Phys. Chem. B*, 2006, **110**, 17987.
66 F. H. Stillinger, *Science*, 1995, **267**, 1935.
67 N. Giovambattista, C. F. Lopez, P. J. Rossky and P. G. Debenedetti, *Proc. Natl. Acad. Sci. U. S. A.*, 2008, **105**, 2274.
68 J. Mittal, P. Shah and T. M. Truskett, *J. Phys. Chem. B*, 2004, **108**, 19769.
69 P. Shah and T. M. Truskett, *Mech. Mater.*, 2006, **38**, 924.
70 T. M. Truskett and V. Ganesan, *J. Chem. Phys.*, 2003, **119**, 1897.
71 A. Attili, P. Gallo and M. Rovere, *Phys. Rev. E*, 2005, **71**, 031204.
72 M. Goldstein, *J. Chem. Phys.*, 1969, **51**, 3728.
73 M. Goldstein, *J. Chem. Phys.*, 1977, **67**, 2246.
74 F. H. Stillinger and T. A. Weber, *Phys. Rev. A*, 1982, **25**, 978.
75 F. H. Stillinger and J. A. Hodgdon, *Phys. Rev. E*, 1994, **50**, 2064.

76 P. G. Debenedetti and F. H. Stillinger, *Nature*, 2001, **410**, 259.
77 W. H. Press, S. Teukolsky, W. Vetterling, and B. Flannery, *Numerical Recipes: The Art of Scientific Computing*, Cambridge University Press, New York, 3rd edn, 2007.
78 J. R. Errington and P. G. Debenedetti, *Nature*, 2001, **409**, 318.
79 L. A. Baez and P. Clancy, *J. Chem. Phys.*, 1994, **101**, 9837.
80 F. W. Starr, F. Sciortino and H. E. Stanley, *Phys. Rev. E*, 1999, **60**, 6757.
81 S. H. Lee and P. J. Rossky, *J. Chem. Phys.*, 1994, **100**, 3334.
82 N. Giovambattista, P. J. Rossky and P. G. Debenedetti, *Phys. Rev. E*, 2006, **73**, 041604.
83 A. R. Leach, *Molecular Modelling: Principles and Applications*, Prentice Hall, Harlow, England, 2nd edn, 2001.
84 M. Schoen and S. Klapp, Nanoconfined Fluids: Soft Matter Between Two and Three Dimensions, in *Reviews of Computational Chemistry*, ed. K. B. Lipowitz and T. Cundari, John Wiley and Sons, New York, 2007, vol. 24.
85 W. Smith and P. Rodger, The Pressure in Systems with Frozen Atoms, in *Collaborative Computational Projects 5 (CCP5)*, 2002, see http://www.ccp5.ac.uk/infoweb/wsmith22/wsmith22.pdf.
86 M. P. Allen and D. J. Tildesley, *Computer Simulation of Liquids*, Oxford University Press, New York, NY, 1987.
87 I. P. Omelyan, *Phys. Rev. E*, 1998, **58**, 1169.
88 H. J. C. Berendsen, J. P. M. Postma, W. F. Vangunsteren, A. Dinola and J. R. Haak, *J. Chem. Phys.*, 1984, **81**, 3684.
89 T. M. Nymand and P. Linse, *J. Chem. Phys.*, 2000, **112**, 6152.
90 A. Y. Toukmaji and J. A. Board, *Comput. Phys. Commun.*, 1996, **95**, 73.
91 D. Frenkel and B. Smit, *Understanding Molecular Simulation: From Algorithms to Applications*, Academic Press, San Diego, CA, 2nd edn, 2002.
92 H. Goldstein, *Classical Mechanics*, Addison-Wesley Pub. Co., Reading, MA, 2nd edn, 1980.
93 F. H. Stillinger and T. A. Weber, *J. Phys. Chem.*, 1983, **87**, 2833.
94 R. A. LaViolette and F. H. Stillinger, *J. Chem. Phys.*, 1985, **82**, 3335.
95 P. G. Debenedetti, F. H. Stillinger, T. M. Truskett and C. J. Roberts, *J. Phys. Chem. B*, 1999, **103**, 7390.
96 S. Sastry, P. G. Debenedetti and F. H. Stillinger, *Phys. Rev. E*, 1997, **56**, 5533.
97 V. K. Shen, P. G. Debenedetti and F. H. Stillinger, *J. Phys. Chem. B*, 2002, **106**, 10447.
98 R. Kumar, J. R. Schmidt and J. L. Skinner, *J. Chem. Phys.*, 2007, **126**, 204107.

